Probing Internal Transport Barriers with Heat Pulses in JET

P. Mantica,[1] D. Van Eester,[2] X. Garbet,[3] F. Imbeaux,[4] L. Laborde,[3] M. Mantsinen,[4] A. Marinoni,[5,*] D. Mazon,[3] D. Moreau,[3] N. Hawkes,[6] E. Joffrin,[3] V. Kiptily,[6] S. Pinches,[7] A. Salmi,[4] S. Sharapov,[6] A. Thyagaraja,[6] I. Voitsekhovitch,[6] P. de Vries,[6] and K.-D. Zastrow[6]

[1]*Istituto di Fisica del Plasma 'P.Caldirola,' Associazione Euratom-ENEA-CNR, Milano, Italy*
[2]*LPP-ERM/KMS, Association Euratom-Belgian State, TEC, B-1000 Brussels, Belgium*
[3]*CEA Cadarache, Association Euratom-CEA, St Paul-lez-Durance Cedex, France*
[4]*Helsinki University of Technology, Association Euratom-Tekes, P.O.Box 2200, Finland*
[5]*Dipartimento di Ingegneria Nucleare, Politecnico di Milano, Milano, Italy*
[6]*Culham Science Centre, EURATOM/UKAEA Fusion Association, Oxon. OX14 3DB, United Kingdom*
[7]*Max-Planck-Institut für Plasmaphysik, EURATOM Association, Garching, Germany*

(Received 10 May 2005; published 7 March 2006)

The first electron temperature modulation experiments in plasmas characterized by strong and long-lasting electron and ion internal transport barriers (ITB) have been performed in JET using ion cyclotron resonance heating in mode conversion scheme. The ITB is shown to be a well localized narrow layer with low heat diffusivity, characterized by subcritical transport and loss of stiffness. In addition, results from cold pulse propagation experiments suggest a second order transition process for ITB formation.

DOI: 10.1103/PhysRevLett.96.095002 PACS numbers: 52.25.Fi, 52.35.Ra, 52.55.Fa

Power modulation experiments are a well-known tool to probe electron heat transport in fusion grade plasmas and have been widely used in conventional L- or H-mode scenarios to assess the physics of turbulence driven transport [1–5]. On the other hand, several key questions remain unsolved on the physics of internal transport barriers (ITBs), i.e., regions where turbulence is quenched and transport greatly reduced [6,7]: for example, regarding the ITB spatial localization, the ITB transport properties and the type of transition mechanism. In this Letter, new results are presented of power modulation experiments in JET plasmas with strong electron and ion ITBs, which provide new evidence on the first two issues. These results are complemented by previously obtained results of cold pulse propagation from the edge into the ITB [8], which are shown to bring information on the type of transition.

The JET tokamak offers good capabilities for perturbative studies of ITBs: the use of lower hybrid (LH) preheat to create a slowly evolving strongly reversed safety factor (q) profile and induce long-lasting ITBs sustained by large neutral beam injection (NBI) power [9], the availability of a space and time resolved electron temperature (T_e) electron cyclotron emission diagnostic, the possibility to use as a transport probe the modulated rf ion cyclotron resonance heating (ICRH) power in mode conversion (MC) scheme, as an alternative to the more commonly used electron cyclotron heating (not available in JET). This deposition scheme, which takes place in D plasmas with ^{3}He concentrations of 10–20% [10,11], provides a source of direct, localized power to electrons, suitable for electron transport studies and already used in JET conventional scenarios [3,4].

JET plasmas with toroidal field $B_T \sim 3.25$–3.6 T, plasma current $I_p \sim 2.6$–2.9 MA ($q_{95} \sim 5$), elongation $k_a \sim 1.75$, triangularity $\delta \sim 0.25$ (averaged lower and upper) and density $n_{e0} \sim 3$–5×10^{19} m^{-3} have been used as targets. LH power ~2–3 MW was applied in the preheat phase ($t = 2$–4 s). Then, from $t = 4$ to 10 s, up to 18 MW of NBI power and 4 MW of ICRH power modulated with half depth at 15–45 Hz with duty cycle ~60% were applied. The ITB is located in the region of negative magnetic shear and lasts several seconds.

Two rf deposition schemes have been explored: (a) ^{3}He concentration ~12%, which led to the best ITB performance (Fig. 1: $T_{i0} \sim 24$ keV, $T_{e0} \sim 13$ keV, $n_{e0} \sim 5 \times 10^{19}$ m^{-3}, at an additional total power level of 15 MW, with an equivalent Q_{DT} [12] ~0.25); (b) ^{3}He concentration ~20%, which allowed the cleanest modulation signals and best transport results (Fig. 2). The rf power deposition has been estimated using both PION [13] and TOMCAT [14] and cross checked with experimental estimates of power ab-

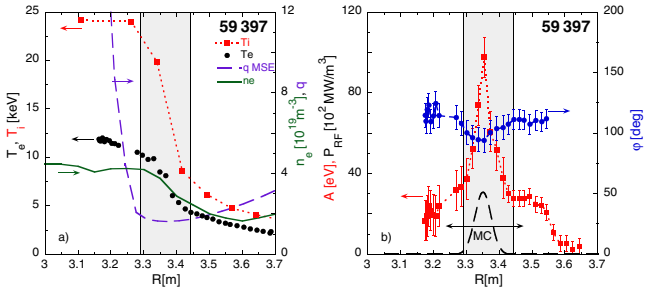

FIG. 1 (color online). (a) Experimental profiles at $t = 8$ s (maximum performance) of T_e, T_i, n_e, and q for shot 59 397 (3.45 T/2.8 MA, ^{3}He ~ 12%, ICRH $f = 33$ MHz). The ITB region is highlighted. Uncertainties for T_e, T_i are in the order of 10%. (b) profiles of Fourier component of A [squares (red online)] and φ [circles (blue online)] at the modulation frequency (15 Hz) during the time interval 6.2–6.48 s. Estimated rf power deposition profiles are also plotted (dashed black line).

sorption using both the break-in slope method and the analysis of high frequency modulation components [15]. At concentrations ~12% and for the high temperatures of the type of shot shown in Fig. 1, about 40–50% of the rf power is directly absorbed by the electrons in the MC region while only a very small amount is directly absorbed on the fast wave. Although central minority ion heating is still high (>50%) at this ^{3}He level, a highly energetic ^{3}He tail can no longer be formed so the power is mainly transferred to bulk ions, leaving MC as the main source of modulated electron heating. At concentrations ~20%, for the type of shot shown in Fig. 2, ion heating is less significant and about 80% of the power is absorbed by the electrons, half via MC at the ion-ion hybrid layer with a localized profile, half in the center via fast wave Landau damping (FWLD) with a broad profile. In both cases the modulated electron source term due to collisional coupling with ions has been estimated by simulations to be completely neglibible (<2%) with respect to the rf modulated source, due to the small amplitude of both T_e and T_i perturbations (< ± 100 eV).

Figures 1 and 2 show steady-state profiles of T_e, T_i, n_e, q and profiles of amplitudes (A) and phases (φ) of the T_e heat wave at the modulation frequency obtained by standard fast-Fourier-transform (FFT) techniques. Only phase values for which the amplitude spectrum shows a clear peak above noise at the modulation frequency have been plotted. The FFT time interval has been limited to few cycles to avoid the rather frequent MHD crashes that characterize ITB plasmas and that would affect the A and φ determination. Error bars on A and φ have been calculated by perturbing simulated T_e time traces with random noise at the experimental level (including statistical noise and noise deriving from small core MHD disturbances) and calculating mean and standard deviation. The noise level assumed for core channels is higher than purely statistical to take into account the presence of small MHD disturbances. In Figs. 1(a) and 1(b) (^{3}He resonance at $R = 3.2$ m) the MC layer is localized at $R = 2.68$ m, mirrored to $R = 3.35$ m, so providing a heat wave generated at the ITB and traveling in two directions away from it. In Figs. 2(a) and 2(b) (^{3}He resonance at $R = 2.72$ m, mirrored to $R = 3.3$ m) the MC layer is localized at $R = 2.36$ m, mirrored to $R = 3.6$ m, so providing a heat wave traveling from outside towards the ITB. In addition, a heat wave from FWLD traveling from center towards ITB is clearly visible in Fig. 2(b). In Fig. 2(c) also A and φ profiles during a time interval in which the ITB is not present are shown, confirming the rf deposition estimates and the smooth nature of heat wave propagation in the absence of the ITB.

Two important questions under debate regarding ITB transport are (i) whether the improved confinement is limited to a narrow layer or rather extends to the whole core region inside the ITB foot; (ii) whether the ITB is a region of stiff transport [4] characterized by a threshold in R/L_{T_e} ($L_{T_e} = -T_e/\nabla T_e$) larger than in conventional plasmas (case 1) or rather a region below threshold where turbulence is suppressed leading to a loss of stiffness (case 2). These two situations are exemplified in Fig. 3 within the assumption of a second order transition scheme for ITB formation. This assumption will be justified later. The concept of phase transition can be applied to ITB formation using as order parameter the electron heat flux, while the plasma response is R/L_{T_e}. First order means that R/L_{T_e} experiences a discontinuity at the transition (see Fig. 5 discussed later) while it stays continuous for a 2nd order transition (Fig. 3). The two cases in Fig. 3 have significant differences for heat propagation, which is regulated by the perturbative (incremental) heat diffusivity $\chi_e^{\mathrm{hp}} = -\partial q_e/n_e \partial \nabla T_e$ (where q_e is the heat flux). χ_e^{hp} is much higher in case 1 with respect to case 2, so one would expect strong damping of the wave in the ITB in case 2, and propagation of the wave through the ITB in case 1.

Regarding question (i), both Figs. 1(b) and 2(b) show sharp discontinuities in the slopes of the A and φ profiles at the foot and at the top of the high ∇T_e region [with a remarkably different behavior with respect to the interval without ITB shown in Fig. 2(c)], indicating that the ITB is indeed a narrow layer with low χ_e embedded in a higher χ_e plasma. In Fig. 1(b) consistency in the change of A and φ slopes is observed, while in Fig. 2(b) amplitudes at the inner ITB side do not drop exactly where phases rise, the reason likely being the presence of a tiny peak due to a small minority heating component at this location. This does not hinder but even strengthens the conclusion that the sharp A drop and φ rise are due to a layer with very low χ_e.

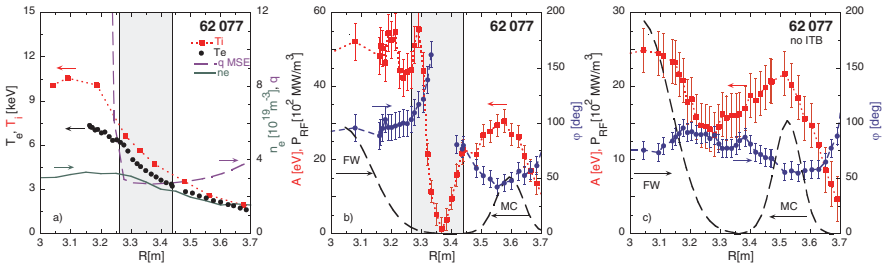

FIG. 2 (color online). (a) Experimental profiles at $t = 5.5$ s of T_e, T_i, n_e, and q for shot 62 077 (3.25 T/2.6 MA, ^{3}He ~ 20%, ICRH $f = 37$ MHz). The ITB region is highlighted. (b) profiles of Fourier component of A [squares (red online)] and φ [circles (blue online)] at the modulation frequency (20 Hz) during the time interval 5.5–5.7 s. Estimated rf power deposition profiles are also plotted (dashed black line). (c) same as (b) for the time interval $t = 8$–9 s, when the ITB has been lost.

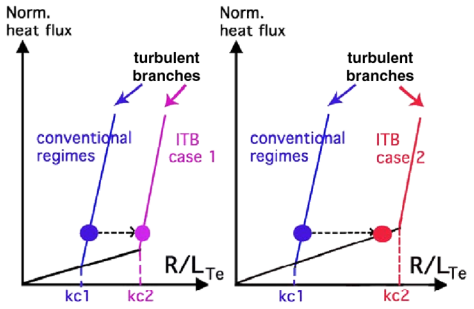

FIG. 3 (color online). Schematic of 2nd order transition for ITB formation. The turbulence threshold is higher than in conventional plasmas. Two situations can be hypothesized, as discussed in the text.

Regarding question (ii), Fig. 2(b) shows that the heat wave is strongly damped when meeting the ITB from either side. This is consistent with a complete loss of stiffness due to the plasma having become fully subcritical with respect to an increased threshold value (case 2). In this case, χ_e does not depend on ∇T_e χ_e^{hp} coincides with the power balance χ_e and is low, the two heat waves are strongly damped and cannot cross the ITB, the phase exhibits a sharp jump. In case (1) instead, corresponding to a plasma in the ITB close to marginality and very stiff, with χ_e^{hp} very large, the two heat waves would propagate fast inside ITB with small phase change and amplitude damping, eventually crossing the ITB and getting superimposed. This is clearly at variance with observations.

Attempts to model the ITB modulation results with various transport models have been carried out [3,16]. More detailed discussion of such modelling effort will be presented in a separate paper [12]. The performance of 1st principle based models is for the moment not satisfactory. Empirical models are in general capable of reproducing the main experimental features using a properly shaped χ_e profile. One example is shown in Fig. 4, using a χ_e critical gradient model (CGM) [4] of the type shown in Fig. 3:

$$\chi_e = \chi_0 + \chi_s T_e^{3/2}\left(\frac{-R\partial_r T_e}{T_e} - \kappa_c\right) H\left(\frac{-R\partial_r T_e}{T_e} - \kappa_c\right). \quad (1)$$

χ_0 quantifies the residual transport (not necessarily neoclassical), χ_s provides the stiffness level, and κ_c is the threshold, assumed to have a square box profile. The ITB is a layer below threshold in a turbulent plasma with significant stiffness level. This crude model is capable of reproducing the basic experimental evidence. Finer refinements are beyond the scope of this Letter.

The oversimplification of the model in Fig. 4 is, however, already evident by considering the asymmetry of slopes in A and φ profiles between the inner and outer portions of the ITB layer in Figs. 1(b) and 2(b). The inner ITB portion has higher slopes, indicating that χ_e^{hp} is not uniform within the ITB, with a lower χ_e^{hp} (i.e., a stronger stabilization of turbulence) in the inner portion and a higher χ_e^{hp} (i.e., partial stabilization) in the outer portion. This corresponds to a situation in which R/L_{Te} is well below threshold on the inner ITB side and stays closer to the threshold on the outer ITB side. In other words the ITB layer gets more fragile in the region near its foot.

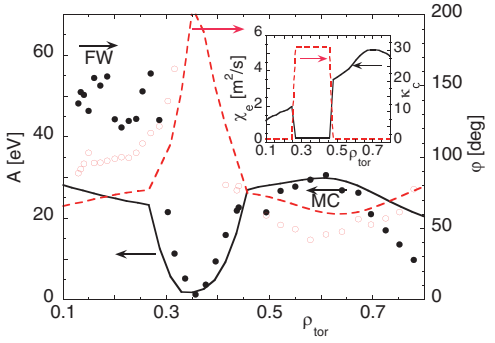

FIG. 4 (color online). Experimental (dots) and simulated using the CGM model [4] (lines) profiles of amplitudes (black full symbols) and phases [open symbols (red online)] at fundamental modulation frequency for shot 62 077. In the inset also the χ_e profile (black full line) used in the simulation is plotted at one time during the modulation ON phase, together with the time constant profile of the threshold κ_c [dashed line (red online)].

This observation is consistent with earlier studies of JET ITBs using cold pulses from the edge induced by Ni laser ablation [8]. Referring to Ref. [8] for all experimental details, we remind here that a cold pulse traveling inward from the edge shows a growth when meeting the ITB foot, and then a strong damping further inside [Fig. 6(a)]. This result is now shown to be an indication in favor of a 2nd order transition scheme for ITB formation (Fig. 3). Within this scheme in fact the cold pulse enhancement in the outer ITB region can be reproduced in terms of a recrossing of the threshold (with associated χ_e increase), due to the enhanced ∇T_e carried by the cold pulse in a region just below the stability threshold. On the other hand, a 1st order transition scheme would not account for the observed cold pulse growth. This scheme is illustrated in Fig. 5, with an S-shaped curve originated by the decorrelation of turbulence eddies due to strong $E \times B$ flow shear, as originally proposed for the edge H-mode barrier formation [17,18], and then de facto extended also to the formation of ITBs. This process is characterized by bifurcation and hysteresis

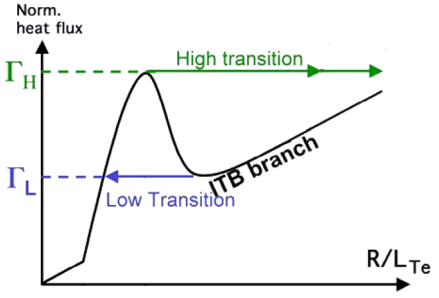

FIG. 5 (color online). Schematic of 1st order transition for ITB formation.

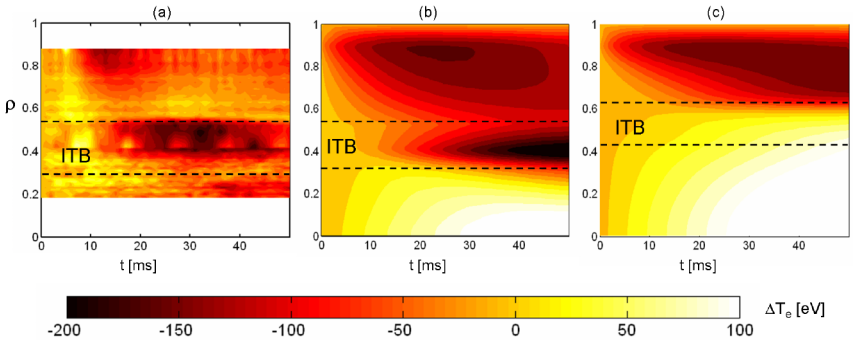

FIG. 6 (color online). Contour plots of ΔT_e during cold pulse in ITB plasma: (a) experimental discharge 51 581; (b) simulated with an empirical 2nd order transition model (as in Fig. 3), (c) simulated with an empirical 1st order transition model (as in Fig. 5). Units of ΔT_e color codes are eV. $t = 0$ ms corresponds to the application of the cold pulse in the edge region.

in the back-transition. Some authors have argued that the critical flux for a 1st order transition should be determined by an equal area (Maxwell) constraint for the backward transition [19] or for both the backward and forward transitions [20], but this does not change our main conclusion. Qualitatively one can see from Fig. 5 that, once bifurcation has taken place and the ITB is formed with transport set to the low transport branch, any further increase in ∇T_e is not a destabilizing factor, so the cold pulse can only be damped by the low transport region. Numerical simulations of the interaction of the cold pulse with the ITB layer have been performed using two empirical models for χ_e reproducing the two types of transitions as in Figs. 3 and 5 [21]. The results are shown in Figs. 6(b) and 6(c). The aim of these simulations is not to achieve a perfect quantitative match of the data, but to show that the two transition schemes yield a very different effect on the cold pulse behavior when meeting the ITB. In the numerical simulations, the radial boundary layer where the transition takes place is modeled by inclusion of a hyper-diffusivity term [22]. In the steady-state phase after the ITB formation, the heat flux at the interface between the 2 regions is consistent with the Maxwell construction. The simulations confirm that cold pulse enhancement can only be reproduced in the 2nd order transition case, when the threshold is overcome in the outer ITB portion and the plasma switches back to the turbulent stiff branch, with consequent χ_e increase. In the 1st order case instead the cold pulse cannot move the plasma away from the ITB branch, and the cold pulse is just damped. Further inside, the cold pulse is damped in experiment and in both simulations, confirming a reduced χ_e^{hp} as indicated by modulation results.

This work was done under the JET-EFDA workprogramme [23]. The views and opinions expressed here do not necessarily reflect those of the European Commission.

*Present address: EPFL, CRPP-Euratom Association, CH 1015, Lausanne, Switzerland

[1] F. Ryter *et al.*, Phys. Rev. Lett. **86**, 2325 (2001).
[2] F. Ryter *et al.*, Plasma Phys. Controlled Fusion **43**, 323 (2001).
[3] P. Mantica *et al.*, in *Proceedings of the 20th International Conference on Fusion Energy, Vilamoura, 2004* [International Atomic Energy Agency (IAEA), Vienna, 2004], EX/P6-18.
[4] X. Garbet *et al.*, Plasma Phys. Controlled Fusion **46**, 1351 (2004).
[5] J. C. DeBoo *et al.*, in *Proceedings of the 20th International Conference on Fusion Energy, Vilamoura, 2004* [International Atomic Energy Agency (IAEA), Vienna, 2004], EX/P6-13.
[6] J. W. Connor *et al.*, Nucl. Fusion **44**, R1 (2004).
[7] X. Garbet *et al.*, Plasma Phys. Controlled Fusion **46**, B557 (2004).
[8] P. Mantica *et al.*, Plasma Phys. Controlled Fusion **44**, 2185 (2002).
[9] X. Litaudon *et al.*, Plasma Phys. Controlled Fusion **44**, 1057 (2002).
[10] M. Mantsinen *et al.*, Nucl. Fusion **44**, 33 (2004).
[11] D. Van Eester *et al.*, in *Recent* ^{3}He *Radio Frequency Heating Experiments On JET*, edited by Cary B. Forest, AIP Conf. Proc. No. 694 (AIP, New York, 2003).
[12] A. Marinoni *et al.*, "Analysis and modelling of power modulation experiments in JET plasmas with Internal Transport Barriers" (to be published).
[13] L.-G. Eriksson *et al.*, Nucl. Fusion **33**, 1037 (1993).
[14] D. Van Eester and R. Koch, Plasma Phys. Controlled Fusion **40**, 1949 (1998).
[15] D. Van Eester, Plasma Phys. Controlled Fusion **46**, 1675 (2004).
[16] P. Mantica *et al.*, in *Proceedings of 31st EPS Conference, London, 2004, Europhysics Conference Abstracts* (European Physical Society, 2004), Vol. 28G, p. 1.154.
[17] F. L. Hinton, Phys. Fluids B **3**, 696 (1991).
[18] P. W. Terry, Rev. Mod. Phys. **72**, 109 (2000).
[19] M. A. Malkov and P. H. Diamond (private communication).
[20] S.-I. Itoh, K. Itoh, and S. Toda, Phys. Rev. Lett. **89**, 215001 (2002).
[21] L. Laborde, D. Mazon, and D. Moreau (private communication).
[22] V. B. Lebedev and P. H Diamond, Phys. Plasmas **4**, 1087 (1997).
[23] J. Pamela *et al.*, *Proceedings of the 20th International Conference on Fusion Energy, Vilamoura, 2004* [International Atomic Energy Agency (IAEA), Vienna, 2004]. (All the members of the JET-EFDA Collaboration appear in the appendix of this paper.)